#6173

DEVELOPMENT AND VALIDATION OF A FINITE ELEMENT CFD ALGORITHM FOR PREDICTION OF ROOM AIR MOTION

A. J. Baker, P. T. Williams and R. M. Kelso
College of Engineering and School of Architecture
The University of Tennessee
Knoxville, TN, USA

SUMMARY

This paper presents theoretical, practical and validation issues on development of a time-accurate, unsteady, stable and mathematically robust finite element CFD algorithm for prediction of room air motion. The incompressible Navier-Stokes equations are closed for the constraint of continuity via a penalty and/or Poisson variable. Their approximate implementation within a CFD theory is *modulo* the discrete divergence operator ∇^h, with intrinsic dispersive (checkerboard) error mode, the control of which is critical to numerical stability.

Upon verification of problem statement well-posedness, the *error* created by constructing *any approximate solution*, to the developed conservation law system, is *extremized* via a Galerkin weak statement. This integral expression formality produces a time-dependent ordinary differential equation (ODE) system, amenable for any integration algorithm. A specific selection produces the terminal non-linear algebraic equation system, which is solved via appropriate quasi-Newton iteration algorithms.

In this paper, the weak statement implementation employs a finite element spatial semi-discretization using low degree tensor product basis functions on 2D quadrilateral- and 3D hexahedron-shaped elements. Time integration is via the second-order accurate trapezoidal rule, and no artificial diffusion is explicitly added. The segregated jacobian, quasi-Newton iteration procedure uses GMRES and PCG sparse solvers. The paper concludes with select 2D and 3D problem statement solutions, comparable to experimental data and/or alternative numerical predictions.

DEVELOPMENT AND VALIDATION OF A FINITE ELEMENT CFD ALGORITHM FOR PREDICTION OF ROOM AIR MOTION

A. J. Baker, P. T. Williams and R. M. Kelso
College of Engineering and School of Architecture
The University of Tennessee
Knoxville, TN, USA

INTRODUCTION

Obtaining an accurate understanding of the distribution characteristics of indoor air is crucial to the development of strategies to efficiently control indoor air quality. The effectiveness of installed ventilation systems is subject to the location of supply outlets, windows, doors, room geometry and exhausts, and interior furnishings, as well as by design of the building heating and cooling systems.

Therefore, one key objective is development of a predictive, computer-based methodology to simulate the movement of indoor air under mixed convection conditions. The mathematical/computational requirement is attainment of accurate *approximate solutions* to the incompressible-thermal, Reynolds-averaged Navier-Stokes equations for flowfields in genuine, three-dimensional room geometries. This field is called "*computational fluid dynamics*" with acronym "*CFD*."

The development and assessment of CFD algorithms, for incompressible or mildly variable density viscous flows, as characterized by sizeable Reynolds number but negligible Mach number, has been underway for almost three decades. The Imperial College group pioneered in the small memory-compatible, semi-implicit steady-state incompressible CFD algorithm "SIMPLE" [1]. Time-accurate, explicit integration CFD procedures were developed in parallel, e.g., the MAC method [2], streamfunction-vorticity and penalty methods, c.f., and the pseudo-compressibility steady-state method [4].

Each of these CFD formulations constitutes the attempt to enable computer-generation of an approximate solution to the governing, non-linear "Navier Stokes (NS)" partial differential equation (PDE) system. This PDE system is considered universally valid; however, many approximations must be made to produce a *computationally tractible* CFD statement. Room air motion flowfields are typically only weakly turbulent, except near the supply diffuser, and non-isothermal, hence a *statistical manipulation* is required to produce the computable "*Reynolds-averaged*" NS form. This introduces a "Reynolds" stress tensor and heat flux vector, requiring a mathematical model for closure. Secondly, room air velocities are low subsonic, hence the air behaves essentially as an incompressible fluid. Pressure thereby becomes decoupled from the thermodynamics, and requires special CFD model handling as a kinematic variable.

Thereafter, a (any) CFD algorithm can at best generate an *approximate solution* to this developed non-linear PDE model system. Numerous theories are available including "finite difference," "finite volume" and "finite element" methodologies, each of which employs a discretization of the PDE statement domain. These methods universally use relatively simple local functions to support the approximate solution, with the result that resolution of phenomena on the scale of the mesh is impossible. Inadequate mesh resolution further enhances the underlying (dominating) dispersive-type error, the control of which is central to stability, both numerical and algebraic.

The terminal expression created by *any* CFD algorithm constitutes a non-linear algebraic equation system requiring matrix iteration to solve. Candidate methods include stationary iterations (Picard, Gauss-Seidel, SOR,...), line relaxation methods (ADI, approximate factorization, ...) and sparse matrix methods (preconditioned conjugate gradient, GMRES, ...). All constitute approximations on a Newton iteration statement, as the general theoretical foundation, and ultimately the resulting CFD code reflects the sum total of all specific approximations and choices.

PROBLEM STATEMENT

A. Reynolds-averaged Navier-Stokes equations

A statistical manipulation of the incompressible Navier-Stokes (INS) equations yields a PDE system amenable to digital computing. The *essence* is to resolve the state variable into a mean component, time-dependent in the large, and a higher-frequency component fluctuation about the mean. The terminal Reynolds-averaged INS system in tensor notation form is

$$\mathcal{L}(\rho_0) \equiv \frac{\partial u_j}{\partial x_j} = 0 \tag{1}$$

$$\mathcal{L}(u_i) \equiv \frac{\partial u_i}{\partial t} + \frac{\partial}{\partial x_j}\left(u_i u_j + \frac{p}{\rho_0}\delta_{ij} + \overline{u_i u_j} - \nu\left(\frac{\partial u_i}{\partial x_j} + \frac{\partial u_j}{\partial x_i}\right)\right) + \frac{\rho}{\rho_0} g_i = 0 \tag{2}$$

$$\mathcal{L}(T) \equiv \frac{\partial T}{\partial t} + \frac{\partial}{\partial x_j}\left(u_j T + \overline{u_j T} - \frac{k}{\rho_0 c_p}\frac{\partial T}{\partial x_j}\right) - s_T = 0 \tag{3}$$

where $\mathcal{L}(\bullet)$ denotes a differential equation including all data. The statistical mean flow variables are (constant) density (ρ_0), velocity vector (u_i), pressure (p) and temperature (T). That density is not uniformly constant is reflected only in the gravity body force term in (2), where g_i is the gravity vector. The material properties of the fluid (air) are kinematic viscosity (ν), thermal conductivity (k), and specific heat (c_p), and s_T is an energy source if present.

The correlated variables (with superscript bar) are Reynolds stress tensor $(\overline{u_i u_j})$ and heat flux vector $(\overline{u_j T})$. The simplest (Boussinesq) closure model constitutes the "constitutive" law form, c.f., [3]

$$\overline{u_i u_j} \equiv \frac{2}{3} k \delta_{ij} - \nu^t \left(\frac{\partial u_i}{\partial x_j} + \frac{\partial u_j}{\partial x_i} \right) + \cdots \qquad (4)$$

where $k \equiv \frac{1}{2} \overline{u_i u_i}$ is called *turbulent kinetic energy*, while ν^t is the unknown turbulent kinematic "*eddy viscosity*." The turbulent Reynolds number definition is $\mathrm{Re}^t \equiv (\nu^t / \nu)$, which is a measure of the flowfield turbulence level (distribution). The turbulent heat flux vector is typically correlated to ν^t via a turbulent Prandtl number $\mathrm{Pr}^t \approx \mathrm{Pr}$. Finally, the k term in (4) is usually "lumped" into the pressure in (2), leaving (4) implemented as a *deviatoric* stress constitutive model.

B. Closure for Incompressibility

Substituting (4) into (2) - (3), using the definition of turbulent Reynolds number, assuming that the turbulent and laminar Prandtl numbers are identical, and non-dimensionalizing by suitable reference length, velocity and kinematic viscosity scales, yields the Reynolds-averaged INS system as

$$\mathcal{L}(q) = \frac{\partial q}{\partial t} + \frac{\partial}{\partial x_j} \left(f_j - f_j^d \right) - s = 0 \qquad (5)$$

along with the continuity equation (1). The state variable $q(x, t)$ in (5) contains the NS dependent variables as the array $\{u_1, u_2, u_3, \Theta, ..\}^T$, where $u_i = u_1 \hat{i} + u_2 \hat{j} + u_3 \hat{k}$ is the non-dimensional velocity vector field and $\Theta = (T - T_{min}) / (T_{max} - T_{min})$ is the potential temperature. The definitions for the kinematic and dissipative flux vectors, and the source array, in (5) are

$$f_j = \begin{Bmatrix} u_j u_1 + P\delta_{1j} \\ u_j u_2 + P\delta_{2j} \\ u_j u_3 + P\delta_{3j} \\ u_j \Theta \end{Bmatrix}, \quad f_j^d = \frac{1 + \mathrm{Re}^t}{\mathrm{Re}} \begin{Bmatrix} E_{1j} \\ E_{2j} \\ E_{3j} \\ \mathrm{Pr}^{-1} \partial \Theta / \partial x_j \end{Bmatrix}, \quad s = \begin{Bmatrix} 0 \\ 0 \\ \mathrm{Ar}\Theta \\ -s_\Theta \end{Bmatrix} \qquad (6)$$

The non-dimensional groups in (6) are,

$$\mathrm{Re} \equiv \frac{UL}{\nu}, \quad \mathrm{Gr} \equiv \frac{g \beta (T_{max} - T_{min}) L^3}{\nu^2}, \quad \mathrm{Pr} \equiv \frac{c_p \rho_0 \nu}{k}, \quad \mathrm{Ar} = \frac{\mathrm{Gr}}{\mathrm{Re}^2} \qquad (7)$$

the kinematic pressure is $P = p / \rho_0 + 2k/3$, and the mean flow symmetric strain rate tensor definition is $E_{ij} = \partial u_i / \partial x_j + \partial u_j / \partial x_i$.

Implementing the continuity constraint (1) is intrinsically connected to the determination of the kinematic pressure P in (6). The penalty model is strictly algebraic, hence the simplest to code-implement with the definition

$$P^p \equiv -\frac{a}{\mathrm{Re}} \frac{\partial u_i^p}{\partial x_i} \tag{8}$$

for $a >> 1$, and iteration superscript "p" denotes the current CFD approximation. The pseudo-compressibility model employs a PDE of the form (5), but is limited to steady-state applications. A Poisson equation form replaces P in (6) with a solenoidal constraint determination satisfying

$$\mathcal{L}(\phi^p) = \frac{\partial^2 \phi^p}{\partial x_j^2} + \frac{\partial u_i^p}{\partial x_i} = 0 \tag{9}$$

The discretized form of both (8) and (9) introduce a dispersive error, *modulo* the mesh measure, producing mesh-wavelength oscillations previously cited as requiring stabilization. An alternative is to replace this solution (P^p) with a (smooth) solution to a pressure Poisson equation, obtainable from (2) using the divergence operator. The resultant PDE is

$$\mathcal{L}(P) = \frac{\partial^2 P}{\partial x_i^2} + \frac{\partial}{\partial t}\left(\frac{\partial u_i}{\partial x_i}\right) + \frac{\partial^2}{\partial x_i x_j}\left(u_i u_j - \frac{\left(1+\mathrm{Re}^t\right)}{\mathrm{Re}}\left(\frac{\partial u_i}{\partial x_j} + \frac{\partial u_j}{\partial x_i}\right)\right) - \frac{\mathrm{Gr}}{\mathrm{Re}^2}\frac{\partial \Theta}{\partial x_g} = 0 \tag{10}$$

Both (9) and (10) require enclosing boundary conditions for well-posedness. The dot product of (2) with the unit vector, pointing outwards from the domain, provides a Neumann boundary condition for (10). The Neumann condition for (9) is homogeneous on all boundary segments where throughflow is specified as data.

FINITE ELEMENT CFD ALGORITHM

A. The Weak Statement

The Reynolds-averaged INS conservation law system contains the state variable $q(\mathbf{x}, t) = \{u_1, u_2, u_3, \Theta, \ldots\}^T$ satisfying (5) - (6) and perhaps an auxiliary variable $q_a(\mathbf{x}, t) = \{\phi, P\}^T$ satisfying a quasi-linear Poisson equation, e.g., (9) and (10). A CFD construction seeks generation of an *approximation* to q and q_a, the associated *error* in which is under the control of the algorithm designer. *Any* such approximation is expressible in the form

$$q(\mathbf{x}, t) \tilde{=} q^N(\mathbf{x}, t) \equiv \sum_{i=1}^{N} \Psi_i(\mathbf{x}, t)\, Q_i(t) \tag{11}$$

The superscript N in (11) distinguishes the *approximate solution*, which is the sum of N products in an assumed *known* function set $\Psi_i(x, t)$ and a set of *unknown* coefficients $Q_i(t)$ that are at most time-dependent. Since (5) is separable initial-value, it is logical to assume that space and time are also separable coordinates. Hence, $\Psi_i(x, t) \rightarrow \Psi_i(x)$ is appropriate, and $Q_i(t)$ then totally supports the time dependence.

Since the "*trial space*" $\Psi_i(x)$ is assumed known (specified), the choice is essentially limitless, e.g., trigonometric functions, Fourier series, Legendre polynomials, Chebyshev polynomials, Lagrange or Hermite interpolation polynomials, etc. The *quality* of $q^N(x, t)$ depends most fundamentally on this choice, but the existence of (11) does not infer how good any specific q^N is. Since q^N is an approximation, it cannot satisfy either (5) or (9)-(10) identically, hence, $\mathcal{L}(q^N) \neq 0$, is a measure of the approximation error $e^N \equiv q - q^N$ associated with any specific q^N.

It makes sense to require that this error be absolutely *minimum* among the specific choices available. The *weak statement* is the functional expression that admits such a condition. The generic weak statement is

$$\int_\Omega w(x, t)\ \mathcal{L}(q^N)\, d\tau \equiv 0 \qquad , \quad \textit{for any } w(x, t) \tag{12}$$

which must hold for *any* "test function" $w(x, t)$, since (12) certainly vanishes when the correct solution $q(x, t)$ is substituted for q^N.

Upon selection of the trial space $\Psi_i(x)$, and the test function $w(x, t)$, completing the integrals in (12) produces an ordinary differential equation (ODE) for (7), and an algebraic system for (9) and (10). Hence, (12) constitutes an *integral transformation* of a system of PDEs, with solution $q(x, t)$, into a (much) larger system of mixed ODEs and algebraic equations written on $Q_i(t)$, the approximation expansion coefficient set. Any discrete time integration method is applicable to the ODE system, e.g., Adams-Bashforth-Moulton, Runge-Kutta, Euler family, leapfrog, etc. Upon implementation, the ODE system becomes an algebraic statement.

One specific development is required for (12) to become a practical numerical recipe; specifically, that (12) must hold for *any* test function must become deterministic. Any known function can be represented by an interpolation; hence, selecting another space of suitable functions $\Phi_i(x)$, *any* interpolation is of the form

$$w(x, t) \simeq w^M(x, t) \equiv \sum_{i=1}^{M} \Phi_i(x)\ W_i(t) \tag{13}$$

where superscript M denotes "interpolation." Once the set $\Phi_i(x)$ is selected, any specific interpolation $w^M(x, t)$ for $w(x, t)$ is distinguishable *only* by the (known) coefficient set $W_i(t)$. Thereby, that (12) must hold for *any* test function can be enforced by requiring this integral to be *stationary* with respect to *all* $W_i(t)$. This *extremum*, the computable weak statement, denoted WS^N, is simply

$$WS^N = \int_\Omega \Phi_i(x)\, \mathcal{L}(q^N)\, d\tau = 0, \quad \text{for any } \phi_i,\ 1 \le i \le M \tag{14}$$

Neglecting some boundary condition theoretical details, M is equal to N, hence (14) produces an ODE system with order equal to the N unknown coefficients $Q_i(t)$ in *any* approximation (11).

While (14) cleanly resolves "*for all* $w(x, t)$" in (12), it has introduced another function set $\Phi_i(x)$ requiring a decision. The *best* choice, in the sense of error, is that the set $\Phi_i(x)$ be *identical* to the trial space $\Psi_i(x)$, which produces the *Galerkin* weak statement

$$GWS^N = \int_\Omega \Psi_i(x)\, \mathcal{L}(q^N)\, d\tau = 0, \quad \text{for } 1 \le i \le N = M \tag{15}$$

Mathematically, the GWS^N is *optimal* in the sense the approximation error in $q^N(x, t)$ is required to be *orthogonal* to every member of the space of functions supporting q^N for *any* choice of trial space. In distinction, the more traditional CFD numerical algorithm construction is called "finite volume (FV)," which reproduces finite differences on regular meshes. In the context of (11)-(13), a FV algorithm for *any* approximation (11) is (13) with $w(x, t)$ the set of all constants. Hence, $\Phi_i(x) \Rightarrow 1$, for all i and (14) becomes

$$FVWS^N = \int_\Omega \mathcal{L}(q^N)\, d\tau = 0 \tag{16}$$

B. Finite element GWS^N semi-discretization

For any approximate solution (11) to (5), the GWS^N terminal form is

$$GWS^N \equiv \int_\Omega \Psi_i(x)\, \mathcal{L}(q^N)\, d\tau = 0, \quad \text{for all } 1 \le i \le N$$

$$= \int_\Omega \{\Psi_i\}\left(\frac{\partial q^N}{\partial t} - s\right) d\tau - \int_\Omega \frac{\partial\{\Psi_i\}}{\partial x_j}\frac{\partial\{n_k\}}{\partial x_j}\left(f_j - f_j^q\right)^N d\tau$$

$$+ \oint_{\partial\Omega_c \cap \partial\Omega} \{\Psi_i\}\left(f_j - f_j^q\right)\hat{n}_j\, d\sigma = \{0\} \tag{17}$$

Note that the last term in (17) provides the venue to analytically impose *any* consistent set of boundary conditions for the NS state variable. The GWS^N is a function (only) of the approximation solution trial space $\Psi_i(x)$ and associated boundary conditions. A *finite element* semi-discretization expresses each $\Psi_i(x)$ as a sum of kth-degree polynomials with compact support. This requires forming a spatial discretization Ω^h,

of the domain Ω on which (5) is valid. The geometrical shape of element domain Ω_e depends on the dimension n of Ω, and on the degree (k) of the local polynomial. The familiar shapes are triangle and quadrilateral in 2D, and the tetrahedron and hexahedron in 3D. Other shapes are specifically derivable, and element sides (or faces, in 3D) may be planar or curved.

The local (FE) polynomials spanning an Ω_e usually have *knots* coinciding with geometrical distinctions, e.g., vertices, mid-sides, etc. State variable member approximation expansion coefficients $Q_i(t)$ are usually assigned to these locations, which are called "*nodes*" of the mesh. It is convention to denote this element-level expression for unknowns as the array (column matrix) $\{Q(t)\}_e$. Similarly, the array of k^{th} degree FE basis polynomials is given the label $\{N_k(\eta_i)\}$, where $\eta_i=\eta_i(x)$ is the normalized intrinsic coordinate system spanning Ω_e.

This "finite element methodology" directly facilitates evaluation of the integrals in the GWS^N, (17), by focussing on one (the *generic*) finite element domain Ω_e within Ω^h. The approximation expression (11) for *any* FE semi-discrete approximation becomes

$$q(x,t) \simeq q^N(x,t) \equiv q^h(x,t) = \bigcup_e q_e(x,t) \qquad (18)$$

where $\Omega^h \equiv \cup_e \Omega_e$, and $\cup_e$ denotes "union" over the FE mesh. The form for $q_e(x,t)$ on any (all) Ω_e is then

$$q_e(x,t) \equiv \{N_k(\eta(x))\}^T \{Q(t)\}_e \qquad (19)$$

and the GWS^N becomes specifically evaluable as

$$GWS^h \equiv \int_{\Omega^h} \Psi_i(x)\, \mathcal{L}(q^h)\, d\tau = 0 \quad , \quad \text{for all } 1 \le i \le N \text{ on } \Omega^h \simeq \Omega$$

$$= S_e \left(\int_{\Omega_e} \{N_k\} \left(\frac{\partial q_e}{\partial t} - s \right) d\tau - \int_{\Omega_e} \frac{\partial \{N_k\}}{\partial \eta_i} \frac{\partial \{\eta_i\}}{\partial x_j} \{f_j - f_j^d\}_e d\tau \right.$$

$$\left. + \int_{\partial\Omega_e \cap \partial\Omega} \{N_k\} \{f_j - f_j^d\}_e \hat{n} d\sigma \right) = \{0\} \qquad (20)$$

All integrals are now performed *only* on Ω_e, and on its boundary $\partial\Omega_e$ when it coincides (intersects, "$\cap$") with $\partial\Omega$, the boundary of Ω. These integrals are easy to evaluate analytically or by numerical quadrature. The net result is creation of a *library* of finite element matrices, one for each term in (5)-(6) as it appears in (20). An FE CFD code is then basically a DO loop of products between element data, and element-independent (FE matrix) data, which is then row-summoned ("*assembled*," denoted "S_e") to form (20). These operations, detailed in [3, 5], communicate the elegance of the GWS^h to a practical code.

Since the time-dependence in any approximation (11), specifically (19), remains continuous, assembling the element-rank expressions in (20) over all Ω_e produces the matrix ODE system

$$GWS^h = [M]\frac{d\{Q\}}{dt} + \{R(Q(t))\} = \{0\} \tag{21}$$

In (21), $[M]$ and $\{R\}$ are global rank square and column matrices, respectively, and $\{Q(t)\}$ is the approximation state variable semi-discretization at the nodes of Ω^h. The *residual* $\{R\}$ is a non-linear function of $\{Q\}$, and contains contributions from *all* terms in (21) except the lead (unsteady) term. Any ODE algorithm utilizes (21) to evaluate derivatives in a Taylor series; for example, selecting the θ-implicit, one-step (Euler/trapezoidal) ODE method, for $t_{n+1}=t_n+\Delta t$ and using (21) yields

$$\{FQ\} = [M]\{Q_{n+1} - Q_n\} + \Delta t\left(\theta\{R\}_{n+1} + (1-\theta)\{R\}_n\right) = \{0\} \tag{22}$$

The GWS^h is similarly formed for any auxiliary Poisson equation, e.g., for the continuity constraint and/or pressure, (9)-(10). Both are quasi-linear in their dependent variable, and the FE procedure employs all developed ingredients except the ODE step. The terminal algebraic equation system is of the form

$$\{FQ_A\} = [D]\{Q_A\} - \{S(Q(t))\} = \{0\} \tag{23}$$

where $\{Q_A\}$ is the mesh nodal array for discretized auxiliary variables ϕ^h and/or P^h, with $\{S(Q(t))\}$ containing the coupling dependence to appropriate members in q^h.

C. Linear algebra, equation solving

The GWS^h FE methodology produces the non-linear coupled algebraic equation systems (22) and (23). Any linear algebra procedure can be interpreted as a quasi-Newton iteration, wherein the jacobian is approximated. The generic Newton iteration algorithm statement for (22) is

$$\left[M + \theta\Delta t\frac{\partial\{R\}}{\partial\{Q\}}\right]\{\delta Q\}_{n+1}^{p+1} = -\{FQ\}_{n+1}^{p} \tag{24}$$

the convergent solution of which yields the $p+1^{st}$ solution estimate

$$\{Q\}_{n+1}^{p+1} = \{Q\}_n + \sum_{i=0}^{p}\{\delta Q\}_{n+1}^{i+1} \tag{25}$$

Here, $p\geq 0$ is the iteration index, and convergence occurs for $\max|\{\delta Q\}^{p+1}| \leq \varepsilon$ for some ε. Any quasi-Newton method amounts to replacement of (24) with some less complicated left hand matrix, and many methods in numerical linear algebra are applicable, along with appropriate insertion of solutions of (23).

D. Theoretical, accuracy and convergence

The selection of trial space $\Psi_i(x)$, $1 \le i \le N$, hence FE trial space basis $\{N_k\}$, is the *absolutely fundamental* choice. Accuracy and rate of asymptotic convergence to the exact solution (algorithm "order") are correspondingly bounded. The NS system contains PDEs of two types, i.e., quasi-linear elliptic and non-linear initial-boundary value statements modulated by a single parameter (Reynolds number). Mathematically rigorous asymptotic error estimates are available only for the linearized forms, c.f., Oden and Reddy [6]. For error defined as $e^h \equiv q - q^h$, the asymptotic error estimate for a GWS^h algorithm (23) for (9) and/or (10) is

$$\| e^h \|_{H^1(\Omega)} \le C\, h_M^k \left(\| f \|_{H^r(\Omega)} + \| g \|_{H^s(\partial\Omega)} \right) \tag{26}$$

In (26), H^p denotes the p-Sobolev norm, defined either on the solution domain (Ω) or its boundary ($\partial\Omega$). Within the norm (notation $\|\bullet\|$), f and g are corresponding *data* of smoothness $r>0$ on Ω and $s \ge 1/2$ on $\partial\Omega$. For sufficiently refined discretizations Ω^h, C is a constant independent of h_M, the extremum mesh measure, and k is the completeness degree of the FE trial space basis $\{N_k\}$.

The companion, linearized asymptotic semi-discrete approximation error estimate for the GWS^h algorithm (21)-(22) for (5)-(6) is [6]

$$\| e^h(n\Delta t) \|_{H^1(\Omega)} \le C_1\ h_M^k \| q(n\Delta t) \|_{H^{k+1}(\Omega)} + C_2\, \Delta t \| Q_0 \|_{H^1(\Omega)} \tag{27}$$

Here, Δt is the integration time step, Q_0 is the interpolation of $q(x, t=0)$ onto Ω^h, and C_1 and C_2 are constants for sufficiently refined Ω^h. Thus, for the exact solution q possessing $k+1$ derivatives that are square integrable, the approximation error will converge in H^1 as the extremum mesh measure h_M to the exponent k, the trial space basis degree.

DISCUSSION AND RESULTS

A. Benchmark Validations

The close-coupled step wall diffuser is an isothermal flow benchmark containing clearly distinguishable solution character as a function of Reynolds number Re. Figure 1a sketches the geometry and illustrates essential flow recirculation patterns as measured experimentally (for h/H=0.485 and H=1.01) for $100 \le Re \le 7500$ based on inlet duct hydraulic diameter [7]. Figure 1b summarizes the measured loci of primary and secondary recirculation region attachment coordinates on the duct symmetry center plane. The flowfield is essentially 2-D for $Re \le 400$, whereupon an axial vortex pair becomes created yielding a fully 3-D flow character with additional upper surface separation region. The flow trips to 3D turbulent at $Re \simeq 1200$, and is fully turbulent for $Re > 6500$, thereupon returning to an essentially 2D character with a single recirculation region. Comparing the associated attachment coordinate

X_1, for the laminar and fully turbulent flowfields, indicates that the associated turbulent Reynolds number is of the order $Re^t=(\nu^t/\nu) \simeq 30$.

Over the range of Re for which the step-wall diffuser flowfield is verified laminar and 2D, both the penalty and continuity constraint GWS^h algorithm solutions, as well as the continuity-exact streamfunction-vorticity formulation, produce essentially identical solutions on an adequate mesh. These solutions are in excellent agreement with the data, Fig. 1c, using an $\Omega^h = 20 \times 70$ axially-nonuniform discretization. The streamfunction and continuity constraint GWS^h algorithms further produce smooth, steady-state 2D solutions to Re = 1000 that are essentially identical, and contain a secondary, and eventually a tertiary, recirculation bubble, c.f., Fig. 1d. These occurrences are in qualitative agreement with the experiment, even though the actual flowfield has become 3D, see Fig. 1b. The penalty GWS^h algorithm solution process, without the addition of artificial diffusion, becomes corrupted by the *modulo* ∇^h dispersive error mode on this mesh, recall the comments with regard to (8).

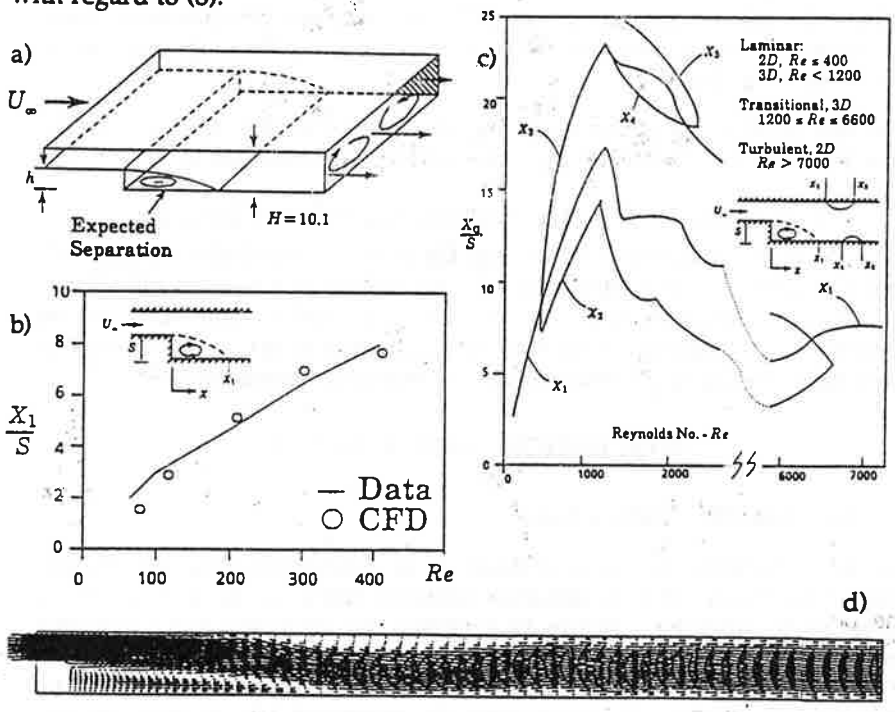

Fig. 1. Close-coupled stepwall diffuser, a) geometry [7], b) GWS^h predictions for X_1, c) flow field character with Re, [7], d) GWS^h 2D simulation at Re=1000.

The fully 3D GWS^h simulation process employs the continuity-constraint with genuine pressure algorithm construction. Figure 2a illustrates the prototypical discretization of the symmetric half-duct containing approximately 20,000 domains Ω_e. For $100 \leq Re \leq 400$, the

associated steady-state solutions are in excellent agreement with the data, Fig. 1b-c. Figure 2b graphs select cutting planes of the computed velocity vector field at Re=400, which appears free from mesh scale oscillation and confirms essential 2-dimensionality of the recirculation region across ~80% of the duct half-span. The GWS^h solution process is now proceeding at Re=500, whereat the experiment confirms the move towards fully 3D flow and creation of a secondary recirculation region on the top wall. This secondary separation region has occurred, and Fig. 2c graphs the complex local flowfield computed in the step-sidewall near-region, with associated initiation of the 3D vortex roll-up and multi-dimensional stagnation points. This computational validation process will continue to Re=1200, in increments of 100, to quantize the associated 3D separation phenomena.

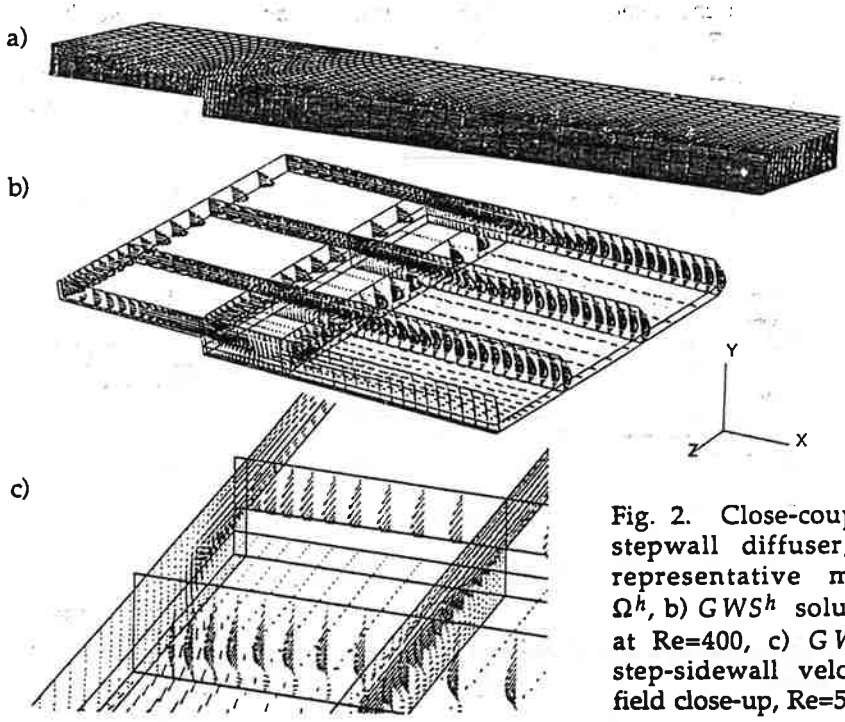

Fig. 2. Close-coupled stepwall diffuser, a) representative mesh Ω^h, b) GWS^h solution at Re=400, c) GWS^h step-sidewall velocity field close-up, Re=500.

The benchmark thermal problem statement is natural convection in a 2D and/or 3D square cavity. The penalty and continuity constraint GWS^h algorithms, on a modestly non-uniform $\Omega^h = 16^2$ mesh, both produce 2D results in excellent agreement with numerical data [8] for $10^3 \leq GrPr \leq 10^6$. The continuity constraint GWS^h 3D algorithm solution, for $GrPr = 10^4$ and $\Omega^h = 16^3$, compares exactly to the 2D solution. (Space limitations prevent inclusion of the associated graphics.)

B. Room Air Motion Predictions

Zhang [9] has measured room air motion in the full scale, essentially 2D room geometry shown in Fig. 3a. The supply duct was diffuserless, as was the room exhaust, and Re $\simeq$ 6000 based on supply duct cross-section

(5 cm) and velocity (350 fpm). For Re~6000, a non-isothermal test was conducted for Ar ~ 0.02. The experimental data confirm both flowfields are unsteady, in the large, with the eye-level supply flow attaching to the ceiling, and separating thereafter as a function of time and Ar.

Figure 3b is a snapshot of the continuity-constraint GWS^h algorithm solution for the isothermal test at $\Delta t \sim 50$ s, for $Re^t=5$, which compares well with the experimental mean flow velocity field,

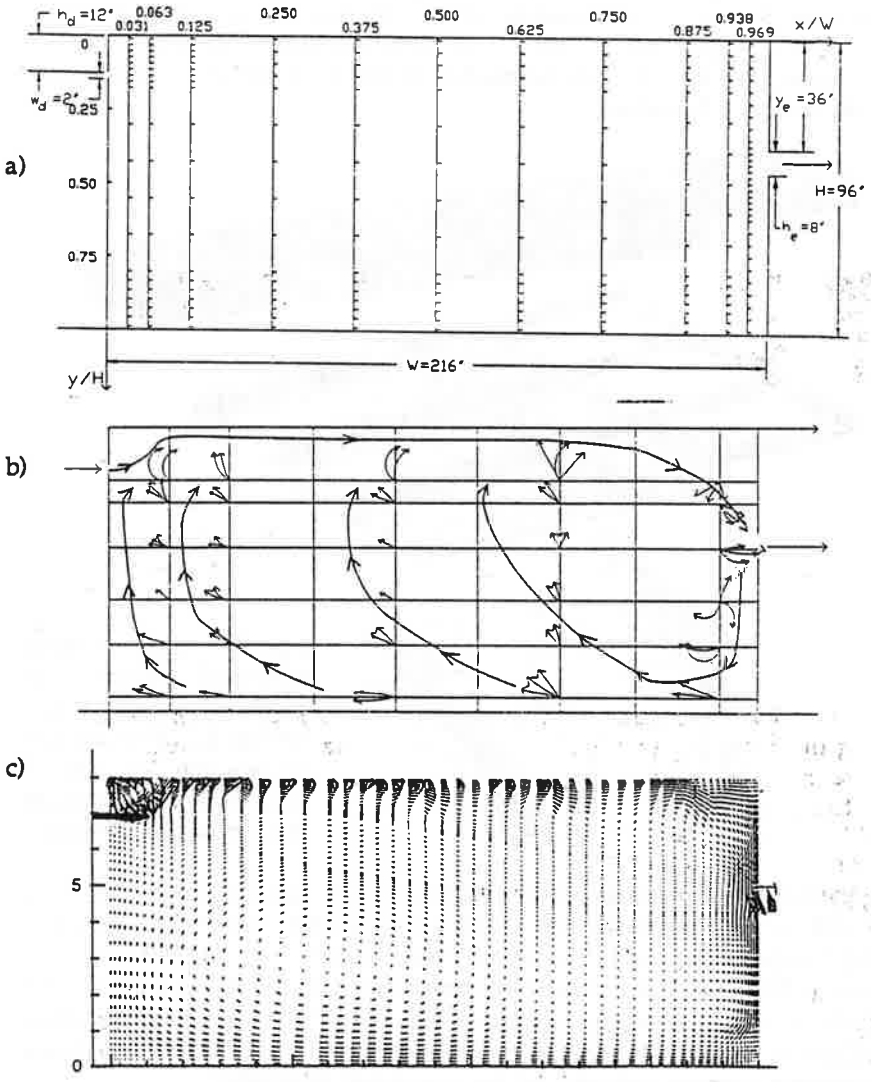

Fig. 3. Full-scale room air motion characterization, a) Univ. Illinois experiment, [9], b) measured velocity field with time-variation illustrated, [9], c) GWS^h prediction, $\Delta t \sim 50s$, $Re^t=5$, $\Omega^h = 50 \times 60$.

Fig. 3c, with its large-scale unsteadiness denoted thereon via the small-scale arrow clusters. The CFD data indicate a relatively long wavelength oscillation in the ceiling jet layer, a firm indication that the separation coordinate will be time dependent. The action of the CFD drag boundary conditions in modulating the wall jet profiles is quite evident. In the near-supply region, the comparison of hot-wire measurements with the CFD prediction of the ceiling jet attachment, Fig. 4a-4b, is quite good.

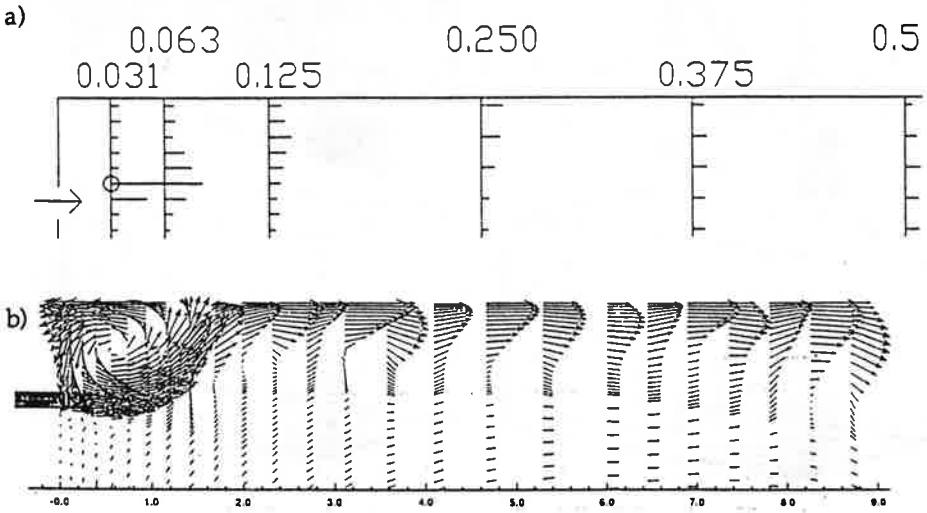

Fig. 4. Full scale room air motion near-field flow characterization, a) experimental hot wire data, [9], b) GWS^h prediction, Δt=50s, Re^t=5, Ω^h = 50 x 60.

Spitter [10] reports data for a full scale 3D room air experiment with strong thermal bouyancy effects. For the air change/hour (ACH) rate of 15, the cold jet injection into a hot room occurs at Re=15,000 and Ar=22. For the ACH=30 case, the jet and room are initially isothermal, Re=30,000 and Ar=4 for the heated walls. The CFD simulations employ the 3D continuity constraint GWS^h algorithm on a mesh containing ~20,000 Ω_e again including discretization into the supply and exhaust ducts. Figure 5 summarizes the essentially steady-state CFD solution for velocity and static pressure distributions for both cases. For the ACH=15 simulation for Re^t=14, the cold jet literally "crashes" onto the floor, hence spreads radially inducing multiple stagnation points and wall thermal boundary layers. The ACH=30 test case CFD simulation at Re^t=29 produces a much different velocity field, while the pressure field is distinguished only by the absence of the floor stagnation region. These predictions are in excellent qualitative agreement with the (relatively sparse) experimental data in [10].

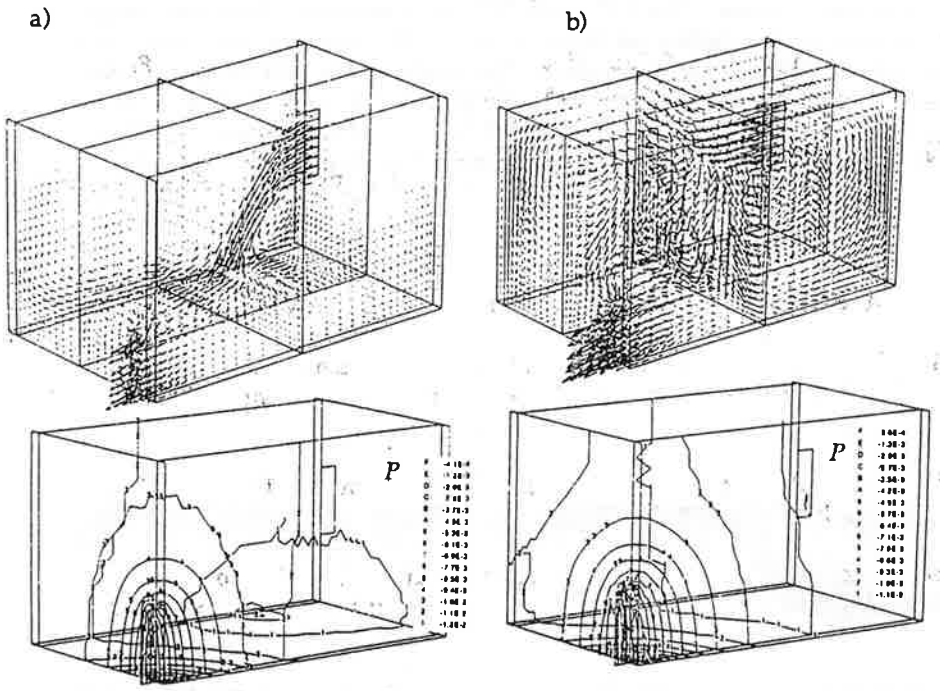

Fig. 5. GWS^h algorithm solution for velocity and pressure distributions, $\Omega^h \sim$20,000, a) ACH=15, Ar=22, Re^t=14, b) ACH=30, Ar=4, Re^t=29.

SUMMARY AND CONCLUSIONS

This paper has presented theoretical, practical and validation issues for a time-accurate, unsteady, stable and mathematically robust weak statement CFD algorithm for prediction of room air motion. The incompressible Navier-Stokes equations appear best closed for the constraint of continuity in 3D via a Poisson variable. For this paper, the weak statement employs a finite element semi-discretization using tensor product basis functions on 3D hexahedron-shaped elements. Time integration is via the second-order accurate trapezoidal rule, and no artificial diffusion is explicitly added. Algorithm performance has been verified for select 2D and 3D benchmark and room air motion problem statements.

ACKNOWLEDGMENTS

Portions of this research have been selectively supported by ASHRAE and the National Science Foundation (NSF) which is gratefully acknowledged. The CFD simulations were conducted in the UT CFD Laboratory, for which we graciously acknowledge longstanding university and industrial sustaining membership support.

LITERATURE

[1] Patankar, S. V., "Numerical Heat Transfer and Fluid Flow," Hemisphere, Washington, DC, 1980.

[2] Amsden, A. A. and F. H. Harlow, "A Simplified MAC Technique for Incompressible Fluid Flow Calculations," J. Comp. Phys., 1970, p. 322-325.

[3] Baker, A. J., "Finite Element Computational Fluid Mechanics," Hemisphere, Washington, DC, 1983.

[4] Chorin, A. J., "A Numerical Method for Solving Incompressible Viscous Flow Problems," J. Comp. Phys., 1967, p. 12-26.

[5] Baker, A. J. and D. W. Pepper, "Finite Elements 1-2-3," McGraw-Hill, New York, NY, 1991.

[6] Oden, J. T. and J. N. Reddy, "An Introduction to the Mathematical Theory of Finite Elements," Wiley, New York, NY, 1976.

[7] Armaly, B. F., F. Durst, J. C. F. Pereira, and B. Schonung, "Experimental and Theoretical Investigation of Backward-facing Step Flow," J. Fluid Mech. 1983, p. 473-496.

[8] deVahl Davis, G., "Natural Convection of Air in a Square Cavity: A Benchmark Numerical Solution," J. Num. Mtd. Fluids, 1983, p. 249-264.

[9] Zhang, J., "A Fundamental Study of Two Dimensional Room Ventilation Flows Under Isothermal and Non-Isothermal Conditions," Ph.D. Dissertation, Univ. Illinois/Urbana, 1991.

[10] Spitler, J. D., "An Experimental Investigation of Air Flow and Convective Heat Transfer in Enclosures Having Large Ventilative Flow Rates," Ph.D. Dissertation, Univ. Illinois/Urbana, 1990.